CROSS SECTION FOR THE ASTROPHYSICAL $^{14}C(n,\gamma)^{15}C$ REACTION VIA THE INVERSE REACTION

Á. Horváth, J. Weiner[1] A. Galonsky, F. Deák[a], Y. Higurashi[b], K. Ieki[b], Y. Iwata[b2], Á. Kiss[a], J.J. Kolata[c], Z. Seres[d], J.von Schwartzenberg[c], H. Schelin[e], S. Takeuchi[b], S. Typel and R.E. Warner[f]

The chain of reactions in primordial nucleosynthesis in the neutron-rich environment of an inhomogeneous big bang involves the reaction $^{14}C(n,\gamma)^{15}C$. Since the halflife of ^{14}C is much larger than the time scale of this nucleosynthesis, it is a potential seed nucleus to produce heavier elements via neutron captures and beta decays along the reaction chains proposed by Kajino, Mathews and Fuller [1]:

$$^{14}C(n,\gamma)^{15}C(\beta^-)^{15}N(n,\gamma)^{16}N(\beta^-)^{16}O(n,\gamma)^{17}O(n,\gamma)^{18}O(n,\gamma)^{19}O.$$

Then A > 20 neon isotopes can be reached in a series of neutron captures and beta decays. Besides this series, ^{14}C can be a starting point of different reaction chains in which the first reaction is, instead of neutron capture, radiative capture of α-particles or protons. Wiescher, Görres and Thielemann [2] have predicted that the dominant reaction among these three is neutron capture. Our experiment measured the cross section for that capture up to $E_n \sim 1.2$ MeV. The main reaction mechanism in that region is thought to be direct capture of p-wave neutrons with E1 radiation to the $1/2^+$ ground state or to the $5/2^+$ first excited state. The relevant energetics are illustrated in Fig. 1.

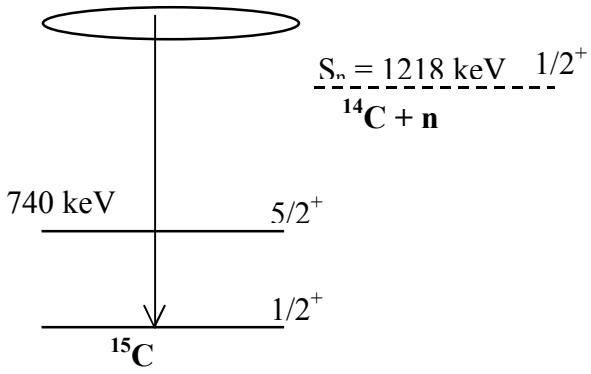

Fig. 1.—The relevant nuclear states and energetics. In the (n,γ) reaction a photon with energy $E_\gamma = S_n + E_{CM}$ is emitted; E_{CM} is the n + ^{14}C energy in its CM system. In the inverse reaction, the γ-ray dissociates ^{15}C into n + ^{14}C with decay energy $E_d = E_{CM} = E_\gamma - S_n$.

The main idea of our experiment was to measure the cross section for the inverse reaction –$^{15}C(\gamma,n)^{14}C$– and apply the principle of detailed balance to determine the $^{14}C(n,\gamma)^{15}C$ cross section. Since it is not possible to produce a ^{15}C target, ^{15}C becomes the projectile, and the virtual photons near a high-Z nucleus become the targets. An advantage of using the inverse direction is that, for E_n > a few keV, phase space factors favor the inverse cross section by 1-2 orders of magnitude in comparison to the direct reaction. This enabled us to determine microbarns of (n,γ) cross section by measuring millibarns of the inverse. Another advantage of using the inverse reaction is that we avoid dealing with a dangerous and expensive ^{14}C target. Two disadvantages are: 1) the need to measure the final state kinematics of each event in order to determine the energy of the photon absorbed, hence, a ^{14}C-n coincidence measurement, and 2) the need to extract the Coulomb part from the measured Coulomb + nuclear dissociation.

Ions of $^{18}O^{6+}$ with E/A = 80 MeV from the K1200 cyclotron produced a variety of nuclear species by projectile-like fragmentation in a Be target. The resulting ^{15}C nuclei at E/A = 35 MeV were selected in the A1200 magnetic fragment separation system operated with a 1% momentum slit and transported to our experiment station about 40 m away. During the experiment the ^{15}C beam intensity averaged ~ 20,000/s and the impurities, mostly Be isotopes, were < 0.1%. Although the primary target was Pb, we also used targets of lower Z-- C, Al, Zn, Sn and Pb-- to enable us to subtract out the nuclear component of the dissociation of ^{15}C into ^{14}C+n. The layout of the experiment is presented in Fig. 2. Its main elements are a ΔE-E fragment detection system [3] on the left side and a pair of neutron walls [4] on the right side. The E detector was segmented, and ~ two of the segments acted as a beam dump for the ^{15}C projectiles.

Without a neutron in coincidence, the fragment detection system could not always separate ^{14}C from ^{15}C. A worst-case example, ^{14}C fragments striking a beam-dump segment, is illustrated in Fig. 3. In that figure the upper part shows the pulse-height spectrum of fragment singles, which were counted simultaneously with coincidence events but downscaled by a factor of 1000. An overwhelming fraction of those events are un-reacted ^{15}C's, but some may be ^{14}C's for which the neutron was not detected. When a neutron coincidence was required, we got the spectrum in the lower part, where the ^{14}C's dominate. The coincidence requirement extracted the needle from the haystack.

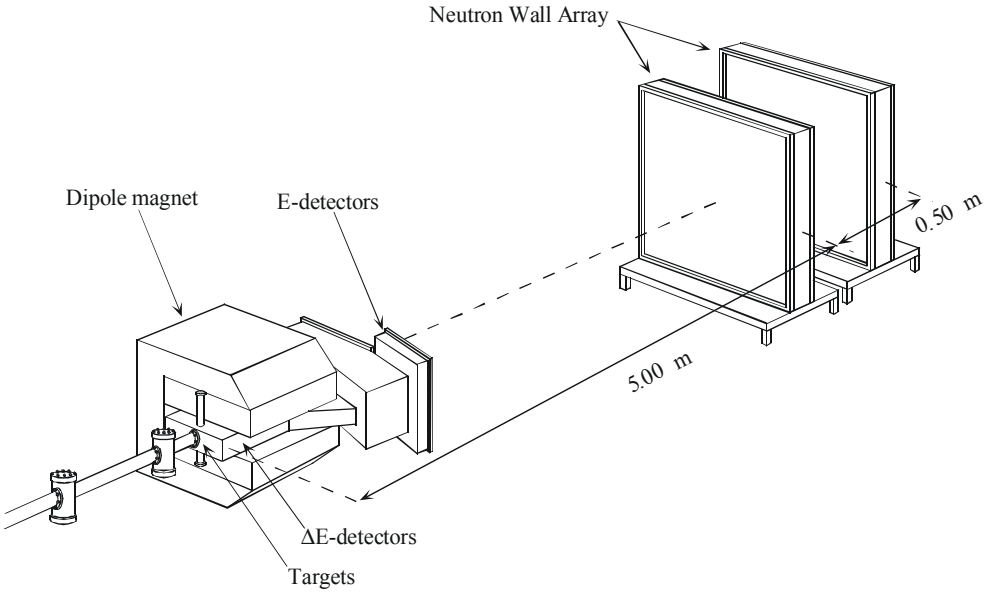

Fig. 2. Layout of the experimental setup. The neutron walls, one behind the other, were placed 5.00 and 5.50 meters from the target at 0°. The fragment detection system consists of silicon strip detectors (ΔE detectors), the dipole magnet and the plastic scintillator array (E-detectors). The ΔE detectors were located 15.2 cm downstream from the target at the entrance of the magnet.

For each ^{14}C–n coincidence event we transformed both velocity vectors to the CM system using Lorentz transformations, and the value of E_d was computed as $\mu v_{rel}^2/2$, where v_{rel} is the relative velocity in the C.M. system, and μ is the reduced mass of ^{14}C + n. In this way we obtained the points and the dashed curves through them in Fig. 4. Removal of the smoothing effect of detector resolution gave the solid curves, the intrinsic (true) cross sections. The Coulomb part of $d\sigma/dE_d$, was determined by its ~ Z^2 dependence from the solid curves in Fig. 4. It is about 95% of the measured total when Pb is the target.

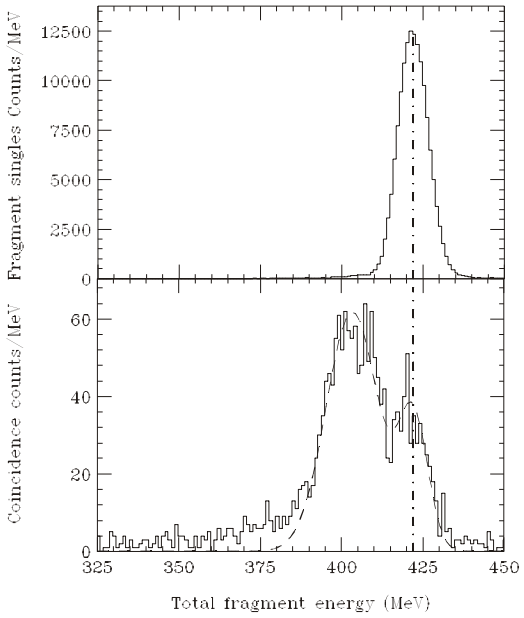

Fig. 3. Spectra of fragments, singles above and coincident with neutrons below. A ^{14}C peak that is invisible in the singles spectrum is dominant in the coincidence spectrum.

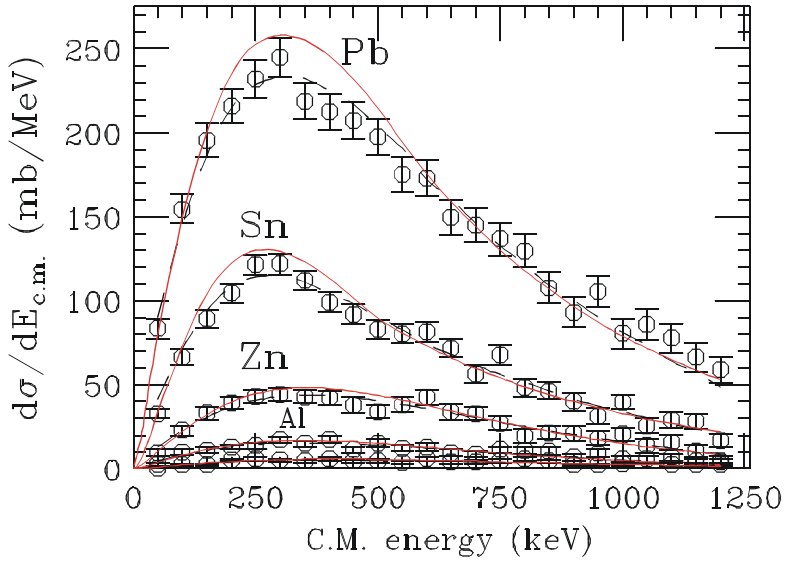

Fig. 4. Dissociation excitation functions for C, Al, Zn, Sn, Pb targets (C at bottom). Open circles are the data with statistical error bars. When the solid lines, the intrinsic (true) functions, are folded with instrumental resolution functions, the dashed-line fits result.

Although we have determined a photon-induced excitation function, $d\sigma/dE_d$ is not the excitation function for $\sigma_{\gamma,n}$. The relationship between those two functions is given by

$$\sigma_{\gamma,n}(E_\gamma) = \frac{E_\gamma}{n(E_\gamma)}\left[\frac{d\sigma}{dE_d}(E_d)\right]_{Coul}, \qquad (1)$$

where $E_\gamma = E_d + S_n$ (see Fig. 1) and $n(E_\gamma)$ [5] is the number function for virtual E1 photons. In principle, virtual photons of multipolarity other than E1 can contribute to ^{15}C dissociation, in particular, E2. Numerical calculations based upon a model [6] showed that the ratio of E2 to E1 dissociation is less than 10^{-4} for $E_d < 1$ MeV.

Using the principle of detailed balance we obtain

$$\sigma_{n,\gamma}(E_n) = \frac{2(2j_{15C}+1)}{(2j_{14C}+1)(2j_n+1)}\frac{k_\gamma^2}{k_{14C+n}^2}\sigma_{\gamma,n}(E_\gamma) = \frac{1}{\mu c^2}\frac{E_\gamma^{\ 2}}{E_n}\sigma_{\gamma,n}(E_\gamma), \qquad (2)$$

where μ is the n-^{14}C reduced mass.

Our measurement of an inverse reaction did not include the inverse of a transition to the excited state because our measurement always started with ^{15}C in the ground state, never in the excited state. Fortunately, both the $E_\gamma^{\ 3}$ dependence of dipole transitions, $[(1.218/(1.218\text{-}0.740)]^3 = 16.5$ at $E_d = 0$, and the measured spectroscopic factors [7], 0.88/0.69 = 1.28, favor the ground state. In addition, the $1/2^-$ continuum states cannot make an E1 transition to the $5/2^+$ excited state. The net result is an estimated correction to the measured part of $\sigma_{n,\gamma}(E_n)$ that increases from 3% at $E_n = 0$ to 16% at $E_n = 1.2$ MeV. The left side of Eq. 2, with this correction added, produced the points in Fig. 5. The two gray lines enclosing the solid one define the region of experimental uncertainty. The dashed curve [2] and the dot-dashed curve [8] are theoretical predictions. The major difference between theory and experiment is the monotonically increasing theoretical curves in comparison to our experimental result, which peaks ~ 0.2 MeV. Both of the calculations used a direct capture model which, due to the p-wave neutron penetrability, gave an initial energy dependence of $E^{1/2}$. Our initial energy dependence is consistent with $E^{1/2}$. For higher energies, however, the increasing penetrability may result in a rising competition between neutron re-emission and γ-ray emission, and that may be responsible for the peak and then the fall-off of our excitation function above 0.2 MeV. Wave function simplifications in the calculations may account for their higher overall magnitudes. The only prior measurement [9] is represented by the point at 23 keV. It falls significantly below our experimental result. In the blowup of the low-energy region on the right side of Fig. 5, we have extrapolated to E = 0 with a ~ $E^{1/2}$ fit to our data. Our fit gives $\sigma_{n,\gamma}$ (23 keV) = 3.2± 0.9 μb, about three times the result of Beer et al. [9].

The reaction rate is expressed in terms of the cross section:

$$R_{n,\gamma}(T) = N_A\langle\sigma v\rangle = N_A\left(\frac{8}{\mu\,\pi(kT)^3}\right)^{1/2}\int\sigma_{n,\gamma}(E)E\exp(-E/kT)dE \qquad (3)$$

We used Eq. 4 and the curves of Fig. 5 to produce corresponding curves of reaction rate *vs.* temperature; they are in Fig. 6. The two theoretical rates [2,8] are fairly close to each other, but they diverge from the experimental result as T increases. The dotted curve is derived from the measured point at 23 keV [9] with the same linear temperature dependence as in the upper dashed curve. At the low temperature side of the figure, the helium-burning region, our results give greater importance to the ^{14}C(n,γ) reaction than was previously demonstrated. The rate of proton capture on ^{14}C [10] is also plotted in Fig. 6. Its temperature dependence is much stronger than the temperature dependence of the neutron capture reaction, and the proton curve intersects all four of the neutron curves, but at rather different temperatures. In the temperature range important for inhomogeneous big bang models, $T_9 = 0.2\text{-}1.2$, the point of intersection determines the relative importance of the two reactions, ^{14}C(p,γ)^{15}N and ^{14}C(n,γ)^{15}C. In Fig. 6 we see that this point varies from $T_9 =$ 0.9 to 1.7

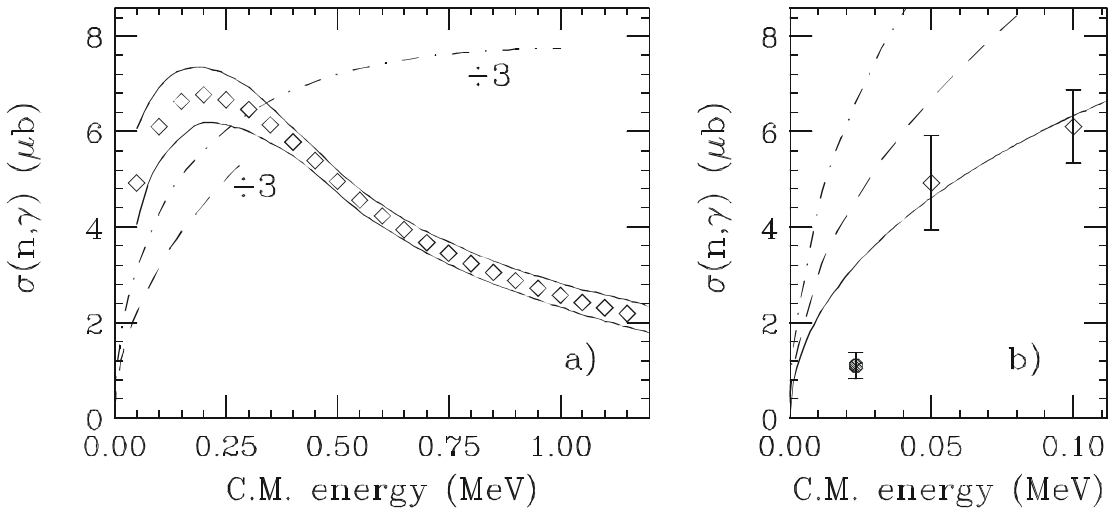

Fig. 5. Excitation function for the $^{14}C(n,\gamma)$ cross section. (a) Points enclosed by two solid curves define the region of the experimental results. Plotted as 1/3 of actual values, the dashed curve is a prediction of Wiescher, Görres & Thielemann [2] and the dot-dashed curve is a prediction of Descouvemont [8]. (b) Blowup of low-energy region showing same theoretical curves, but not ÷3, the result of Beer at al. [9] (solid point) and our lowest-energy points (diamonds) with a kinematical fit (solid curve).

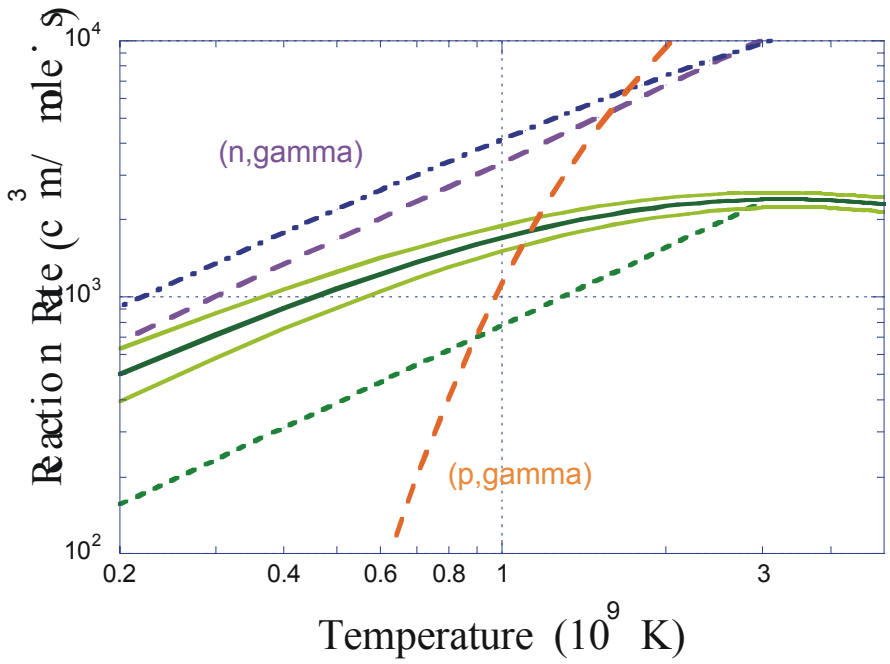

Fig. 6 Reaction rates. Solid line enclosed by the gray error curves represents results of the present experiment. Dot-dashed curve [8], upper dashed curve [2] and the (p,γ) curve [10] result from calculations. Dotted curve is derived from measured $\sigma_{n\gamma}$ at 23 keV by Beer et al. [9].

We thank Thomas Rauscher and Pierre Descouvemont and Hendrik Schatz for helpful comments.

a. Eötvös Loránd U., Budapest, Hungary
b. Rikkyo, Tokyo, Japan; U.
c. U. of Notre Dame
d. KFKI, Budapest, Hungary
e. CEFET, Curitiba, Brazil
f. Oberlin College, Oberlin, OH

Present Addresses:
1. Physics Department, U. Cal., Berkeley
2. National Inst. Radiological Sciences, Chiba, Japan

References

1. T. Kajino, G.J. Matthews and G.M. Fuller, Ap.J. **364**, 7 (1990).
2. M. Wiescher, J. Görres and F.K. Thielemann, Ap.J. **363**, 340 (1990).
3. J.J. Kruse, A. Galonsky, C. Snow, E. Tryggestad, J. Wang, K. Ieki, Y. Iwata, and P.D. Zecher. Nucl. Instr. and Meth Phys. Res. **A** (2001) to be published.
4. P.D. Zecher, A. Galonsky, JJ. Kruse, S.J. Gaff, J. Ottarson, J. Wang, F. Deák, Á. Horváth, Á. Kiss, Z. Seres, K. Ieki, Y. Iwata and H. Schelin. Nucl. Instr. and Meth. Phys. Res. **A401**, 329 (1997).
5. C.A. Bertulani and G. Baur, Phys. Rep. **163**, 302 (1988).
6. S. Typel and G. Baur, Phys.Rev. C 64, 024601 (2001).
7. J.D. Goss, P.L. Jolivette, C.P. Browne, S.E. Darden, H.R. Weller, R.A. Blue. Phys. Rev. C12 1730 (1975).
8. P. Descouvement, Nucl. Phys. A **675**, 559 (2000).
9. H. Beer, M. Wiescher, F. Käppeler, J. Görres and P.E. Koehler. Ap.J. **387**, 258 (1992).
10. L.H. Kawano, W.A. Fowler, R.W. Kavanagh. & R.A. Malaney, Ap.J. 372, 1 (1991).